Received: 11 May 2020 | Revised: 3 July 2020 | Accepted: 9 July 2020

DOI: 10.1002/jbm.b.34692

Check for updates

ORIGINAL RESEARCH REPORT

Society For Biomaterials | WILEY

Harnessing electrospun nanofibers to recapitulate hierarchical fibrous structures of meniscus

Xiaoyu Wang[1] | Jingjing Zhu[1] | Binbin Sun[1] | Qiu Jin[1] | Haiyan Li[1] | Changlei Xia[2] | Hongsheng Wang[1] | Xiumei Mo[1] | Jinglei Wu[1,3]

[1]Key Laboratory of Science and Technology of Eco-Textile, Ministry of Education, College of Chemistry, Chemical Engineering and Biotechnology, Donghua University, Shanghai, PR China

[2]Co-Innovation Center of Efficient Processing and Utilization of Forestry Resources, College of Materials Science and Engineering, Nanjing Forestry University, Nanjing, PR China

[3]Department of Plastic and Reconstructive Surgery, Shanghai Key Laboratory of Tissue Engineering, Shanghai Ninth People's Hospital, Shanghai Jiao Tong University School of Medicine, Shanghai, PR China

Correspondence
Jinglei Wu, Department of Bioengineering, Donghua University, 2999 North Renmin Road, Shanghai, 201620, PR China.
Email: jw@dhu.edu.cn

Funding information
Donghua University, Grant/Award Number: 2232019D3-20; National Natural Science Foundation of China, Grant/Award Number: 31900949; Science and Technology Commission of Shanghai Municipality, Grant/Award Numbers: 18490740400, 19440741300

Abstract

The meniscus has complex biomechanical functions endowed by the hierarchical fibrous structure of its extracellular matrix (ECM), which plays a central role in protecting the knee joint. However, it is challenging to recapitulate the ECM structure of the meniscus. Herein, we used electrospinning to prepare various scaffolds with distinct nanofibrous structures to approximate that of the heterogeneous ultrastructure of meniscus ECM. Our results showed that adjusting the deposition manner of nanofibers during electrospinning could effectively manipulate the architectures of resulting scaffolds. This approach led to electrospun scaffolds with random or aligned fibrous structures that reassemble the surface or superficial layers of the meniscus. We also showed that assembly of electrospun nanofibers into yarn-like configurations replicates the circumferentially aligned fibrous bundles of the inner part of the meniscus. These scaffolds exhibited distinct fibrous anisotropies and mechanical properties. In vitro studies indicated good cytocompatibility of scaffolds, especially, the yarn scaffold supported considerable meniscus cell infiltration. The meniscus cells, in turn, enhanced the mechanical properties of scaffolds. Taken together, these data imply that electrospun scaffolds may have potential in enhancing meniscus repair and regeneration.

KEYWORDS

decellularized meniscus ECM, electrospinning, meniscus tissue engineering, nanofibrous scaffolds

1 | INTRODUCTION

The meniscus is a crescent-shaped fibrocartilaginous tissue located between the femoral condyle and the tibial plateau and provides mechanical support and stabilizes the knee joint. Meniscal tears are one of the most frequent types of injuries in knee joints and represent an important osteoarthritis factor.[1,2] The periphery of menisci is moderately vascularized and has some self-healing capability, while spontaneous healing of tears occurred in the avascular inner zone of menisci is not found.[3] Currently, meniscectomy (partial or total) is the most popular treatment for meniscal tears. However, resection of meniscal tissue results in destructive effects on knee joints, leading to serious osteoarthritis complications.[4,5] Other arthroscopic approaches such as sutures, screws, arrows, staples, and darts have been exploited to treat avascular meniscus tears.[6] These treatments temporarily relieve pain and reduce instability of knee joints, but they are not capable of restoring meniscus or recovering meniscus function and fail to prevent degenerative knee joint changes in the long term. Thus, there is an unmet need for advanced therapeutic approaches to treat diseased or injured menisci.

The meniscus is a dense and thick tissue composing of densely compacted collagen fibrillar bundles (Figure 1a) ranging from nano- to micro-scale. Specifically, the surface and superficial layers are composed of 100 nm collagen fibrils, while the circumferential collagen

 © 2020 Wiley Periodicals LLC

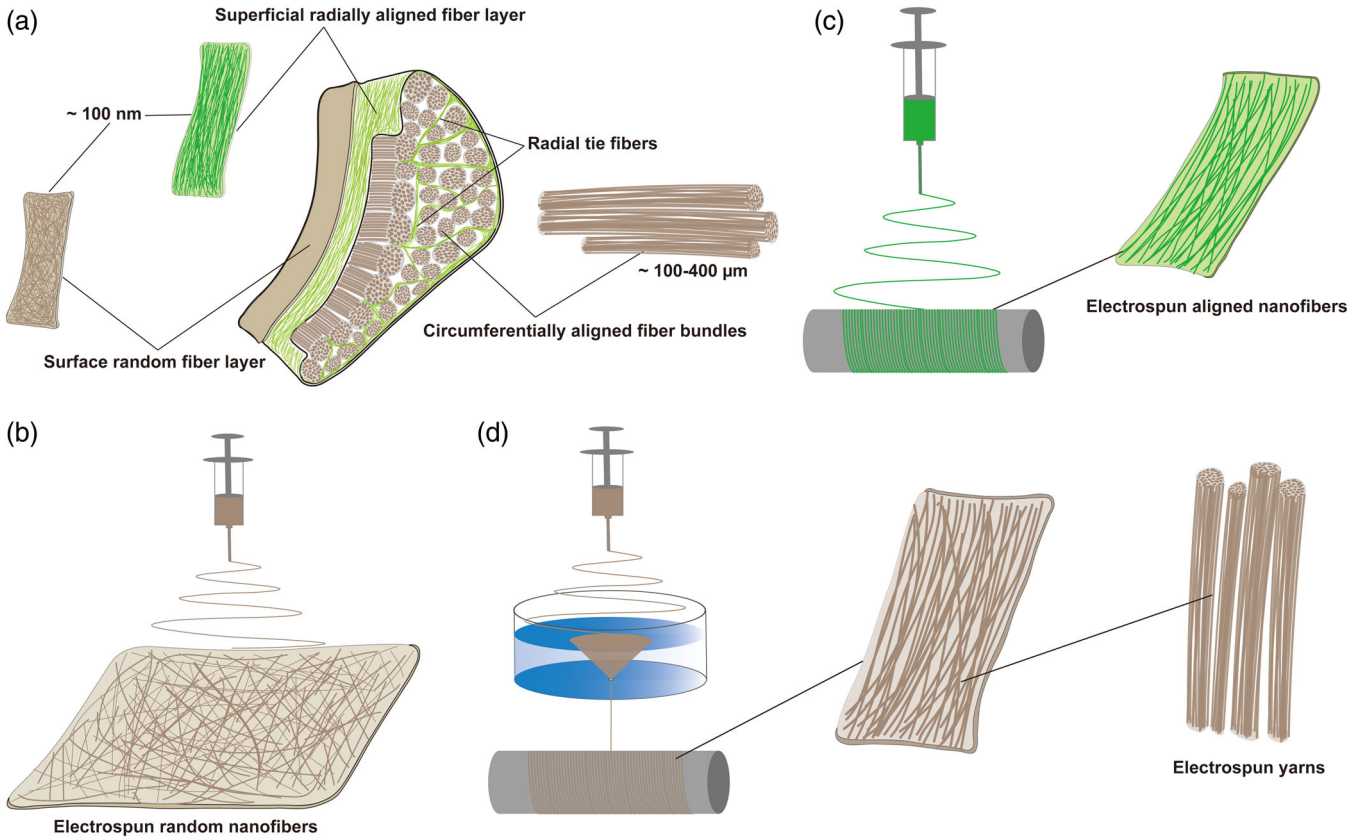

FIGURE 1 Overview of electrospinning to prepare scaffolds for recapitulating the hierarchical fibrous structures of meniscus ECM. The surface of the meniscus is composed of a thin layer of randomly oriented nanofibers (a). Underneath the surface layer, there is a superficial layer constitutes of radially aligned nanofibers. The major structure of the meniscus provides tensile strength is the circumferentially aligned fiber bundles. Electrospun nanofibers are collected either by a flat metal plate (b), a rotating mandrel (c), and a dynamic liquid system (d) to prepare random, aligned, and yarn scaffolds, respectively, to replicate the hierarchical ECM ultrastructure of the meniscus

fibrillar bundle sizes on the range of 100–400 μm.[7,8] The major building blocks of meniscus are circumferentially aligned collagen fibrillar bundles that account for adequate tensile strength to resist vertically converted forces along the circumferential direction. The meniscal superficial layer mainly consists of radially aligned collagen fibrils, which encapsulate the circumferential collagen bundles and emanate into the meniscus interior as radial tie-fiber sheets with the role of tying up circumferential bundles.[9] The top surface of the meniscus has a randomly oriented collagen fibril layer, which is tribological equivalent to its counterpart articular cartilage and intimately contacts with cartilage to protect the kneejoint. This unique hierarchical fibrous structure confers adequate mechanical strength of menisci, whereas it increases the difficulty in recapitulating the native meniscal ECM architecture through engineering approaches. Therefore, an essential prerequisite for fabricating ideal meniscus scaffolds is to recapitulate the distinctive layer fibrous structures of the meniscus.

Electrospinning is a versatile and cost-effective technique to produce nanofibrous mats with tunable mechanical strength comparable to native tissues and has been widely utilized to prepare nanofibrous scaffolds for a variety of regenerative applications. Tuan[10,11] and Mauck[12-15] groups elaborately demonstrated the great potential of electrospun scaffolds for meniscus tissue engineering. Electrospun nanofibrous scaffolds with random and aligned nanofibrous organizations appeared to properly mimic the top layer and superficial layer, respectively.[16] In contrast, replication of the circumferential collagen fibril bundles of the meniscus via electrospinning is rarely reported. Previously, we have reported nanofibrous yarn scaffolds prepared by electrospinning with a dynamic liquid collecting system.[17,18] These scaffolds possess aligned nanofibrous yarns, rough surface, and large pores, which allow full-depth cell infiltration and have shown promise in a variety of tissue engineering applications.[17,19-22] Morphologically, the nanofibrous yarn highly reassembles the fibrous structure of circumferentially oriented collagen fibril bundles of menisci. We, therefore, hypothesized that the nanofibrous yarn scaffold might be an excellent candidate for recapitulating circumferential fibril bundles of menisci.

Recapitulation of the distinctive ultrastructural features of menisci could be achieved by manipulating the nanofiber deposition behaviors during electrospinning, incorporating scaffolds with meniscus-specific biochemical cues could further improve the biomimetics of scaffolds. Recently, decellularized meniscus ECM (dmECM) has been extensively reported for meniscus repair and regeneration.[23-25] It contains meniscus-specific biochemical compositions that are advantageous for the maintenance of fibrocartilaginous phenotypes.[26] However, dmECM is a dense material and cannot be feasibly

dissolved by commonly used solvents for electrospinning. We have previously reported an injectable dmECM hydrogel, in which dmECM was enzymatically digested into a solution.[27] After digesting and lyophilizing, the solubilized dmECM becomes a porous sponge, like reconstituted collagen, and can be easily dissolved for electrospinning. Gao et al demonstrated that the electrospinning of pure dmECM results in a fragile nanofibrous membrane, while the addition of polycaprolactone (PCL) could significantly enhance the flexibility and biological performance the resulting hybrid scaffold.[28] These results indicate that electrospinning of dmECM/synthetic polymers might be an effective approach to prepare scaffolds that are structurally and biochemically mimicking the meniscal ECM structure.

The objective of this study is to prepare a series of electrospun scaffolds and evaluate their capacity for meniscus repair and regeneration. We electrospun poly(L-lactic acid-co-caprolactone) (PLLA-CL)/dmECM solution and collected the as-spun nanofibers by a flat plate (Figure 1b), a rotating mandrel (Figure 1c), and a dynamic liquid system (Figure 1d) to obtain scaffolds that reassemble the distinctive fibrous structures of the surface, superficial, and deep layers of the meniscus (Figure 1a), respectively. Primary meniscus cells isolated from rabbits were utilized to determine the cytocompatibility, cellular infiltration, and biomechanics of these scaffolds.

2 | MATERIALS AND METHODS

2.1 | Decellularization of menisci

Knee joints of Yorkshire pigs (~80 kg weight) were obtained from a local slaughterhouse and transported to the laboratory in an ice bath. Menisci were dissected from knee joints and decellularized as previous reports[26,27] with minor modifications. Menisci were sectioned into thin slices (~1 mm thickness) and pulverized into 1–2 mm^3 particles. Pulverized meniscal samples were agitated in 1 mg/ml pepsin (Sigma-Aldrich, St. Louis, MO) in 0.02 M hydrochloric acid (HCl) (Aladdin Bio-Chem Technology Co., Shanghai, China) solution at room temperature for 48 hr to form a viscose solution. Gradient centrifuge was performed to remove undissolved particles, nuclear remnants, and cellular residues at 4 °C as follows: 2,000 rpm for 10 min to remove the pellet; 6,000 rpm for 10 min to remove the pellet; 11,000 rpm for 30 min to collect the pellet of slurry dmECM. Samples were then frozen at −80 °C overnight, lyophilized, and stored at −20 °C for further use.

2.2 | Preparation of electrospun scaffolds

PLLA-CL (LA: CL = 75:25, Jinan Daigang Biomaterial Co., Jinan, China) and dmECM were separately dissolved in 1,1,1,3,3,3-hexafluoro-2-propanol (HFIP) (Da-Rui Co. Ltd., China) to yield 12% (wt/vol) solutions and then mixed at the PLLA-CL: dmECM ratio of 9:1 for electrospinning. The PLLA-CL/dmECM mixture was fed at 1 ml/hr and charged with a 10 kV voltage to generate nanofibers. Various collectors were used to collecting nanofibers to obtain scaffolds mimicking distinct meniscal ECM structures as depicted in Figure 1. A flat metal plate (15 × 15 cm) was used to collect fibers to form randomly orient nanofibrous scaffolds with a similar ultrastructure of the surface layer of the meniscus (Figure 1b). To mimic the aligned fibrous structure of the superficial layer, electrospun nanofibers were collected by a rotating mandrel (100 mm diameter, 3,000 rpm) to obtain aligned nanofibrous scaffolds (Figure 1c). Nanofibrous yarn scaffolds were prepared via dynamic liquid electrospinning as we previously reported[17,18] to recapitulate the circumferentially aligned ECM structure of the meniscus. Electrospun nanofibers were twisted into yarns through a water vortex and finally collected by a rotating mandrel (100 mm diameter, 60 rpm) to form nanofibrous yarn scaffolds (Figure 1d), which were immersed in deionized water and frozen at −80 °C and lyophilized for further use.

2.3 | Characterization of scaffolds

The morphology of scaffolds was visualized by scanning electron microscopy (SEM). Samples were sputter-coated with gold and observed by a Phenom XL Desktop scanning electron microscope (Phenom, Netherlands) at an accelerating voltage of 5 kV. Compositional analysis was conducted by Fourier transform infrared spectroscopy (FTIR). PLLA-CL, dmECM, and scaffolds were analyzed using an attenuated total FTIR (Nicolet-760, Madison, WI) over the range of 800–2,600 cm^{-1}. The crystalline phase of samples was analyzed by an X-ray diffractometer (XRD, D8 Discover, Bruker AXS, Billerica, MA). Thermogravimetric analysis (TGA) of PLLA-CL, dmECM, and scaffolds was performed using a Libra 209F1 TGA (Selb, Germany) at a scan rate of 20°C/min under inert atmosphere.

The contact angle of scaffolds with a water droplet was measured by an SL200A contact angle analyzer (Solon Tech., Shanghai, China). A droplet of 5 μl deionized water was dropped carefully onto the surface of each scaffold and photographed to calculate the contact angle. A line tangent to the surface of the water droplet was constructed and used to determine the contact angle of scaffolds (n = 4).

Although many studies reported high tensile strengths of electrospun scaffolds in the dry state, the mechanical performance of scaffolds in wet state is more physiologically relevant.[28-30] Thus, we determined the mechanical properties of scaffolds both in dry and wet states. Samples were incubated in PBS at 37 °C for 24 hr prior to wet test. Rectangular samples (10 × 50 mm) were mounted in the grips of a uniaxial testing machine (Instron 5567, Norwood, MA) with a 200 N load cell and tested at a crosshead speed of 5 mm/min until failure. Ultimate tensile strength (UTS) was calculated from the maximum load before failure and Young's modulus was calculated as the slope of the initial 5% linear portion from the stress–strain curve (n = 4 for each group).

2.4 | Isolation and expansion of meniscus cells

Meniscus cells were isolated from rabbit menisci as a previous report.[28] Knee joints of New Zealand white rabbits (4-week old) were collected

from a sacrificed experimental cohort at the School of Medicine, Shanghai Jiao Tong University. Menisci were dissected from knee joints through an aseptic surgery, diced into 1–2 mm^3 particles, and digested with 2 mg/ml collagenase II (Sigma-Aldrich, St. Louis, MO) at 37°C for 2 hr. Single cell suspension was centrifuged, passed through a 70 μm cell strainer, and then preplated in a 10 cm petri dish in high glucose DMEM medium supplemented with 10% fetal bovine serum and 1% penicillin/streptomycin antibiotics placing in an incubator (37 °C, 95% humidity, and 5% CO_2). Meniscus cells proliferated and merged on the surface of the petri dish within approximately 14 days. Cells were then trypsinized and passaged for expansion up to two passages. The medium was changed twice weekly for both cell isolation and expansion.

2.5 | Cell seeding

Electrospun scaffolds were punched into either 22- or 14-mm discs to fit 12-well or 24-well plates, respectively, disinfected with 70% ethanol, and washed thoroughly with PBS prior to cell seeding. Meniscus cells at 80% confluence were detached with trypsin, centrifuged, and resuspended in medium. Aliquots of appropriate cell suspensions were seeded onto the surface of scaffolds. The seeding density of cells on the scaffolds is 5×10^4 cells/cm^2. Cell-seeded scaffolds were transferred to a 37 °C incubator for 1 hr to allow cell attachment and then added with extra medium for culture up to 5 weeks. Samples were harvested at predesignated time points and tailored to pieces with appropriate sizes for further analyses.

2.6 | Viability, proliferation, and morphology of meniscus cells

Cell viability and proliferation were determined by live/dead staining and CCK-8 assay per manufacturer's instructions, respectively (n = 3). Cell morphology was visualized by SEM. At day 1, week 3, and week 5, cell-seeded scaffolds were harvested and fixed with 4% paraformaldehyde and stored at 4°C. Samples were dehydrated with gradient ethanol and lyophilized for SEM observation.

2.7 | Histological analysis

Paraformaldehyde fixed cell-seeded scaffolds (14-mm diameter) were embedded in paraffin and sectioned to 7 μm thick. Sections were stained with hematoxylin and eosin (H&E) and imaged with a microscope (DMi 8, Leica, Germany).

2.8 | Mechanical properties of cell-seeded scaffolds

Mechanical properties were quantified via a uniaxial tensile test as described previously.[30,31] After 3 and 5 weeks, cell-seeded scaffolds (22-mm diameter) were tailored 5 × 20 mm strips along the fiber direction for the test. Uniaxial tensile test was performed as aforementioned (n = 4). Cell-free scaffolds were maintained under the same condition as cell-seeded scaffolds for comparison (n = 4).

2.9 | Statistical analysis

Data were expressed as mean ± SD. Student's t test or one-way analysis of variance (ANOVA) with Tukey's post hoc multiple comparisons were used to analyze significance where appropriate. A significant difference was considered at $p < .05$.

3 | RESULTS

3.1 | Scaffold properties

Porcine menisci were pulverized, digested by pepsin, and centrifuged for decellularization. Previously, we and other groups proved the effectiveness of this method for meniscus decellularization.[26-28,32] The obtained dmECM could be fully dissolved in HFIP and was miscible with PLLA-CL for electrospinning. The electrospun PLLA-CL/dmECM nanofibers were collected by three different devices, namely, a flat metal plate (Figure 1b), a rotating mandrel (Figure 1c), and a dynamic liquid system (Figure 1d) to prepare random, aligned, and yarn scaffolds, respectively, which recapitulate the hierarchical fibrous structures of the native meniscus (Figure 1a). Macroscopically, the random (Figure 2a) and aligned (Figure 2b) scaffolds presented a smooth surface, in contrast, the yarn scaffold showed a rough texture with visibly aligned fibrous structures (Figure 2c). SEM images further revealed the difference of surface texture of random (Figure 2d) and aligned (Figure 2e) scaffolds had a dense surface composed by densely compacted nanofibers, while the yarn scaffold exhibited a loose surface of aligned yarns with grooves (Figure 2f). Cross-section images depicted dense fibrous structures of random (Figure 2g) and aligned (Figure 2h) scaffolds, in which laminated nanofibrous layers were observed. The cross-sectioned yarn scaffold also showed evident laminated layers (Figure 2i) with a distance between layers was much greater than that of random and aligned scaffolds.

The FTIR spectra of electrospun scaffolds and raw materials are presented in Figure 3a. The absorption of amide I and amide II in dmECM appeared at 1,628 and 1,546 cm^{-1}. These peaks in random, aligned, and yarn scaffolds had a weak shift to the high wavenumbers of 1,651 and 1,547 cm^{-1}, respectively, indicating the presence of dmECM in electrospun scaffolds. The XRD patterns of electrospun scaffolds are shown in Figure 3b. The sharp diffraction peaks of raw PLLA-CL at 2θ = 16.6 and 19 can be corresponded to crystallographic planes, indicating the highly crystalline structure of L-lactyl unit sequences. In contrast, dmECM exhibited a completely amorphous phase as revealed by the absence of prominent crystalline peaks. The main characteristic peak of PLLA-CL weakened, and the other peak totally disappeared in the electrospun scaffolds. This indicates that

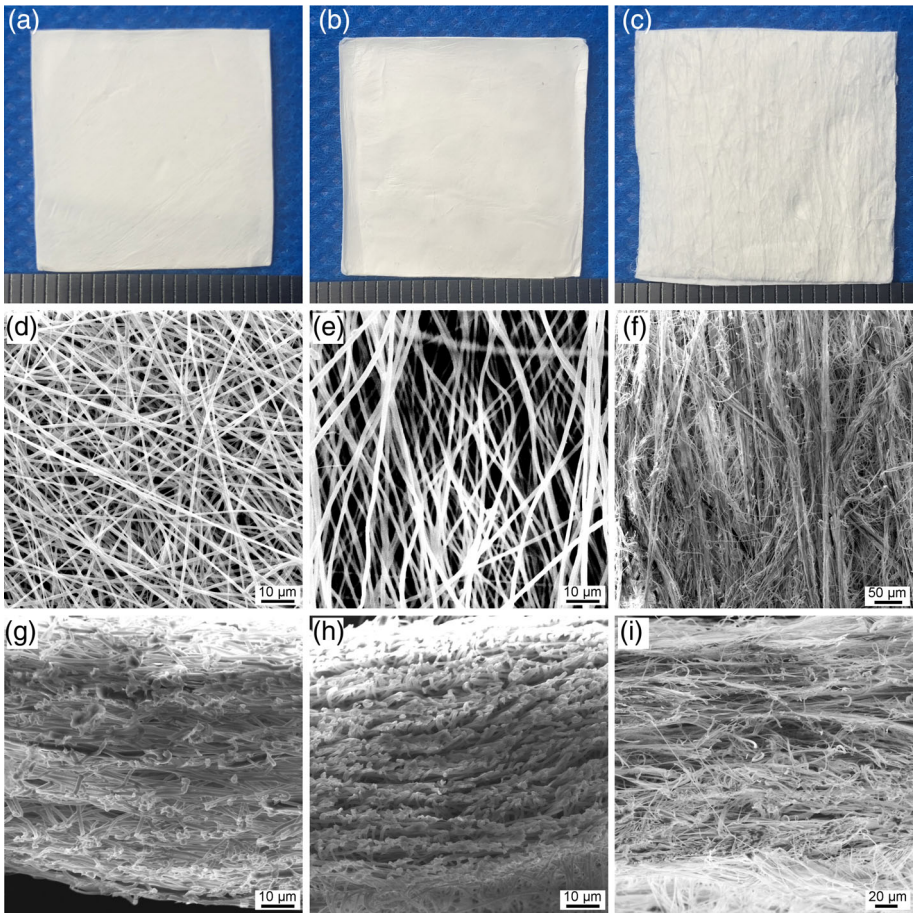

FIGURE 2 Ultrastructure of electrospun scaffolds. Digital images reveal smooth surface textures of the random (a) and aligned (b) scaffolds, while the yarn scaffold (c) has a rough surface with the evident fibrous organization. SEM images confirm the densely compacted nanofibers of the random (d) and aligned (e) scaffolds. Aligned yarns composed of nanofibers confer a loose surface of the yarn scaffold (f). Cross-section images also indicate the dense nanofibrous configuration of random (g) and aligned (h) scaffolds. In contrast, the yarn scaffold shows laminated layers with less compacted fibrous structures (i)

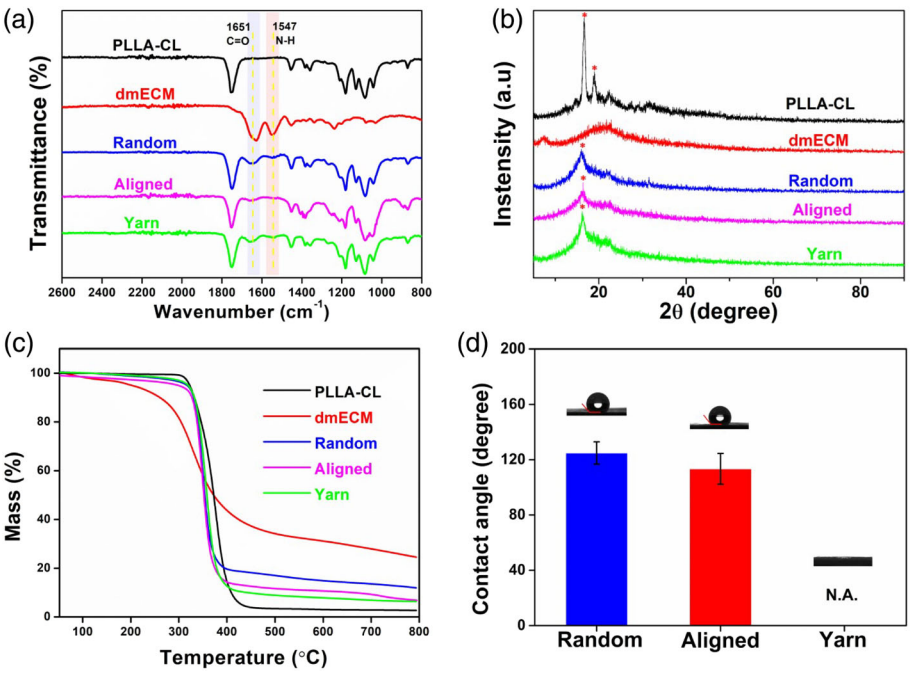

FIGURE 3 Chemical and physical properties of electrospun scaffolds. FTIR (a), XRD (b), TGA (c), and contact angle (d). Asterisks indicate crystalline peaks. N.A., not applicable

dmECM affects the arrangement of PLLA-CL chains and decreases its ordered structure, which is resulted from the molecular interactions between PLLA-CL and dmECM. These data confirm the incorporation of dmECM into electrospun scaffolds. In addition, it is worth noting that both the FTIR spectrum and XRD pattern of the yarn scaffold are almost identical to that of the random and aligned scaffolds, implying

that the dynamic water system did not compromise the incorporation of dmECM into the yarn scaffold.

TGA technique was used to assess the thermal stability of electrospun scaffolds (Figure 3c). The initial degradation temperature of dmECM is significantly lower than that of PLLA-CL. Moreover, the initial degradation temperature of electrospun scaffolds slightly decreased due to the incorporation of dmECM. This result suggests that the incorporation of dmECM reduces the thermal stability of electrospun scaffolds.

The hydrophilicity of electrospun scaffolds was determined by measuring the water droplet contact angle as shown in Figure 3d. PLLA-CL is known to have a hydrophobic surface property, the addition of natural materials such as collagen, gelatin, and silk fibroin will increase the hydrophilicity of the resulting scaffolds. While in the current study, both the random and aligned scaffolds were generally hydrophobic as revealed by contact angles between 110° and 120°. This might be attributed to the relatively lower amount of dmECM in electrospun scaffolds. The water droplet disappeared immediately when dropped onto the surface of the yarn scaffold. We infer that this phenomenon is associated with its porous surface texture that allows considerable water uptake.

The uniaxial tensile strengths of scaffolds were determined both in dry and wet state. The stress–strain curves of random (Figure 4a), aligned (Figure 4b), and yarn (Figure 4c) scaffolds in wet state were lower than that of their corresponding scaffolds in dry state. Hydration lowered the yield points (Figure 4a–c) and slightly decreased the UTSs of scaffolds (Figure 4d). While the UTSs of scaffolds in wet state (8 ± 1 MPa, 15 ± 4 MPa, and 7 ± 1 MPa for the random, aligned, and yarn scaffolds, respectively) were lower than their corresponding scaffolds in dry state (9 ± 3 MPa, 18 ± 2 MPa, and 9 ± 1 MPa for the random, aligned, and yarn scaffolds, respectively), no significant difference was observed (Figure 4d). In contrast, hydration increased the breaking strains of the random (91 ± 13% vs. 114 ± 9%) and aligned (29 ± 5% vs. 79 ± 11%) scaffolds but not the yarn scaffold (84 ± 4% vs. 81 ± 2%) (Figure 4e). Hydration significantly decreased Young's moduli (Figure 4f) for three scaffolds (25 ± 5 MPa vs. 107 ± 33 MPa for the random scaffold, 66 ± 24 MPa vs. 246 ± 35 MPa for the aligned scaffold, 34 ± 13 MPa vs. 72 ± 14 MPa for the yarn scaffold).

3.2 | Cell proliferation and morphology

The viability and proliferation of meniscus cells were assessed by live/dead staining and CCK-8 assay, respectively. At day 1, individual cells could be observed on the surface of scaffolds with predominate viable cells (green) and a few dead cells (red) (Figure 5a–c). Cells with polygonal shape dominated on the random scaffold (Figure 5a), while cells showed predominate spindle shape and organized along the fibrous direction on the aligned (Figure 5b) and yarn (Figure 5c) scaffolds. After 3 weeks, an evident increase in cell population and a low level of dead cells were observed (Figure 5d–f). Meniscus cells maintained the polygonal shape on the random scaffold (Figure 5d), while they presented elongated shapes and organized along with the fiber directions of the aligned (Figure 5e) and yarn (Figure 5f) scaffolds. From weeks 3 to 5, cells retained high viability on the scaffolds (Figure 5g–i). In line with these qualitative results, CCK-8 assay also demonstrated a great increase in cell number after 3 weeks, and cells continued to proliferate thereafter to 5 weeks (Figure 5j). At each time point, there was no significant difference in the proliferation rate between different scaffolds (Figure 5j).

SEM images (Figure 6) reveal the morphology and organization of meniscus cells on the scaffolds. At day 1, meniscus cells exhibited a similar flatten morphology and spread out well both on the random

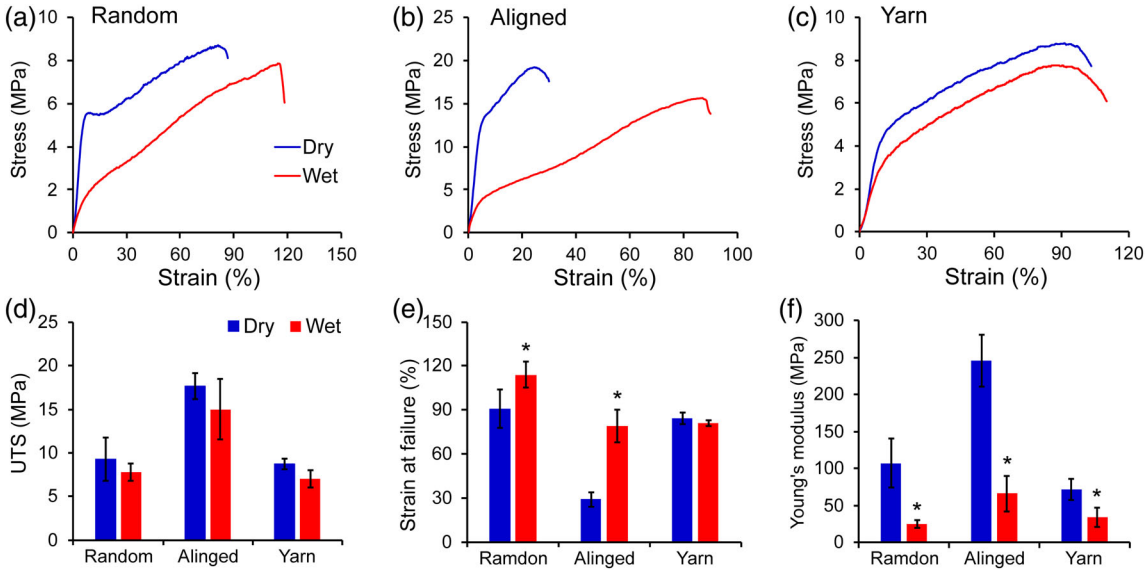

FIGURE 4 Mechanical properties of electrospun scaffolds. Typical stress–strain curves of random (a), aligned (b), and yarn (c) scaffolds with UTS (d), strain at failure (e), and Young's modulus (f). Unpaired student's *t* test, Asterisk "*" indicates $p < .05$ versus dry

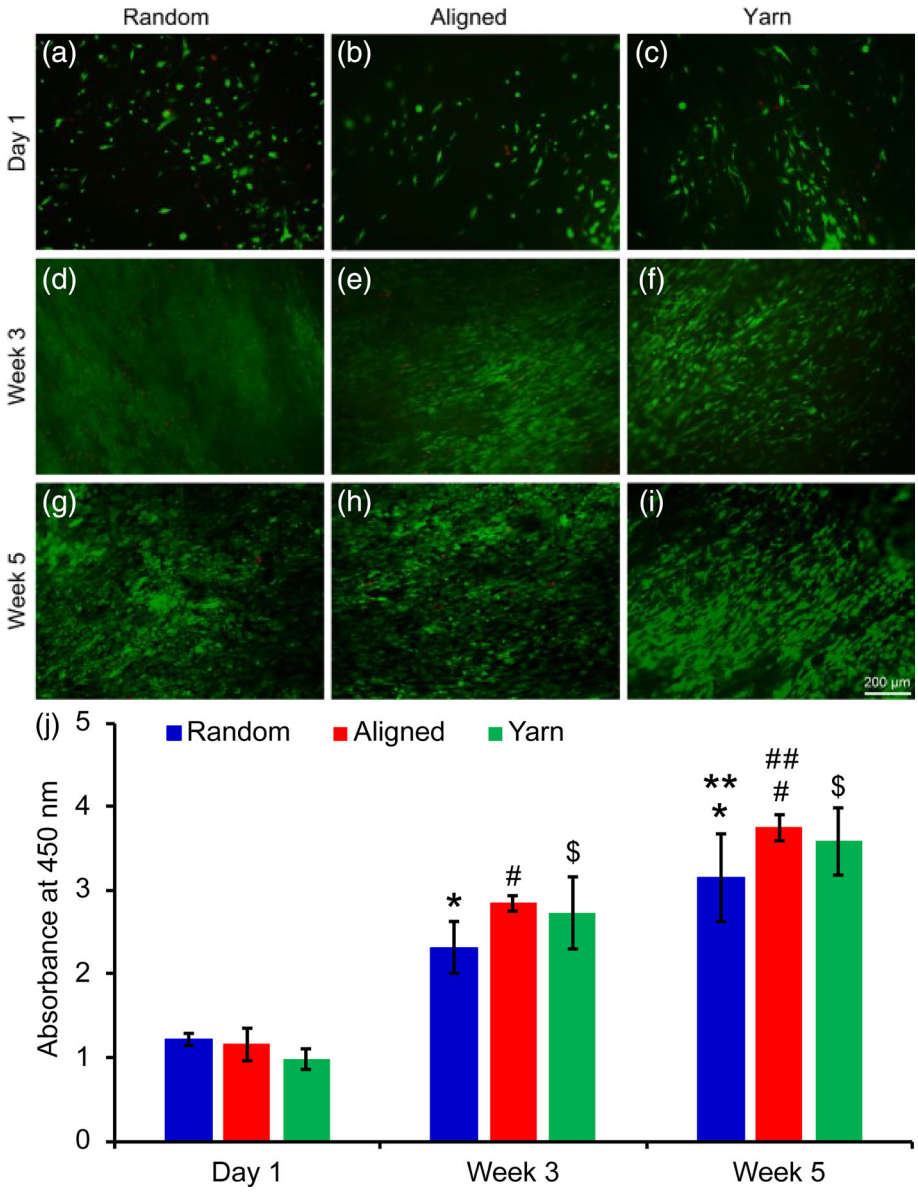

FIGURE 5 Viability and proliferation of meniscus cells with electrospun scaffolds. Live/dead staining (a-i) indicates good cytocompatibility of electrospun scaffolds as live cells (green) predominate, only a few dead cells (red) are observed up to 5 weeks. Meniscus cells show no organization on the random scaffold (a, d, and g), while they proliferate along with the fiber direction on the aligned (b, e, and h) and yarn (c, f, and i) scaffolds. CCK-8 assay demonstrates a steady increase in cell numbers up to 5 weeks (j). One-way ANOVA with Tukey's post hoc test, $p < .05$; *, #, and $ versus day 1; **, ##, and $$ versus week 3

(Figure 6a) and aligned (Figure 6b) nanofibrous scaffolds, they elongated along the fiber direction on the aligned scaffold but not on the random scaffold. Cells were less spread with relatively small cell area evident stereoscopic vision and attached to the yarn scaffold with at day 1 (Figure 6c). Thereafter, increased coverage of meniscus cells on scaffolds was observed from week 3 (Figure 6d–f) to week 5 (Figure 6g–i). This disparity indicates that meniscus cells could recognize and respond to various surface textures of nanofibrous scaffolds.

3.3 | Cell infiltration

Cross-sections of cell-seeded constructs were stained with H&E to visualize the infiltrative behaviors of meniscus cells (Figure 7). As revealed by H&E staining, meniscus cells were restricted to proliferate on the surface of random (Figure 7a,d) and aligned (Figure 7b,e) scaffolds by their dense nanofibrous structures up to 5 weeks. In contrast, the yarn scaffold exhibited relatively loose fibrous structures with homogeneous pores, in which meniscus cells progressively infiltrated into the scaffold and showed increased down growth from week 3 (Figure 7c) to week 5 (Figure 7f).

3.4 | Mechanical properties of cell-seeded constructs

The mechanical properties of cell-seeded constructs were determined using a uniaxial tensile test. Cell-seeded constructs had higher curves over their corresponding cell-free constructs at weeks 3 and 5 (Figure 8a–c). The cell-seeded random scaffold had comparable UTS with the cell-free random scaffold at week 3, but it showed significantly greater UTS than the cell-free scaffold at week 5 (Figure 8d). Meniscus cells did not change the UTS of the aligned scaffold (Figure 8e), while cells increased the UTS of the yarn scaffold at weeks

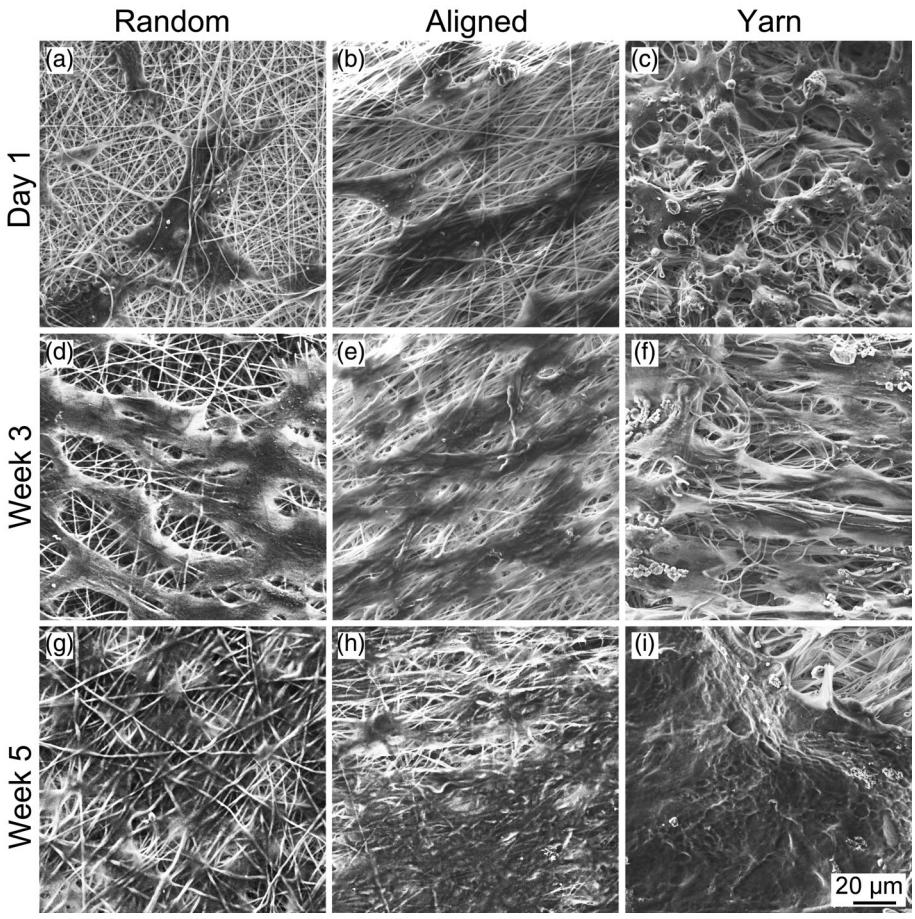

FIGURE 6 SEM images of meniscus cells on electrospun scaffolds. Meniscus cells adhere firmly to the random (a) and aligned (b) scaffolds and exhibit a flatten morphology at day 1. Cells are not fully attached to the yarn scaffold due to its porous fibrous structure at day 1 (c). Increased numbers of cells are observed at week 3 (d–f) and form a confluent layer on the surface of scaffolds at week 5 (g–i)

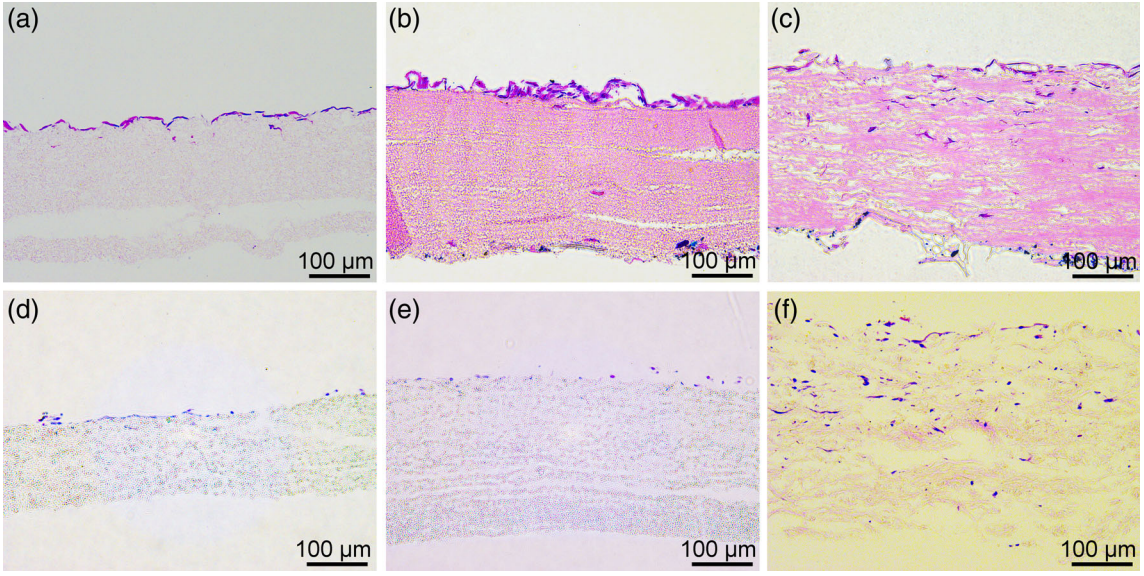

FIGURE 7 Histological analysis of meniscus cells on electrospun scaffolds. H&E staining reveals cell distribution on the scaffold from week 3 (a–c) to week 5 (d–f). Meniscus cells are gathering on the surface of random (a and d) and aligned (b and e) scaffolds, while they progressively infiltrating into the yarn scaffold (c and f)

3 (5.9 ± 0.5 MPa vs. 5.0 ± 0.6 MPa) and 5 (6.3 ± 0.5 MPa vs. 5.3 ± 0.6 MPa) (Figure 8f). Meniscus cells had negligible effects on the breaking strains of the random and aligned scaffolds up to 5 weeks (Figure 8g–i), but they significantly increased the elongation of the aligned scaffold at week 5 (82 ± 8% vs. 67 ± 9%). All cell-seeded constructs showed decreased moduli with time during 5-week

culture (Figure 8j–l). Cell-seeded constructs experienced less loss of moduli than that of cell-free scaffolds, indicating a critical role of meniscus cells in maintaining the elastic properties of constructs.

4 | DISCUSSION

Repair and regeneration of injured menisci continue to be one of the most challenging arthroscopic surgeries. Biomimetic scaffolds provide appropriate microenvironments for cell proliferation and tissue remodeling and might pave a new avenue to meniscus repair and regeneration. In this proof-of-concept study, we demonstrate the capacity of electrospinning technique in creating scaffolds that not only contain meniscus-specific components but also resemble the hierarchical fibrous structures of the meniscus. These scaffolds exhibit distinct anisotropies, mechanical properties, and fibrous densification, which profoundly affect the cell infiltration and biomechanics of cell-seeded constructs.

We began this work with a particular interest in replicating the hierarchical fibrous structures of the meniscus. Recently, Li et al

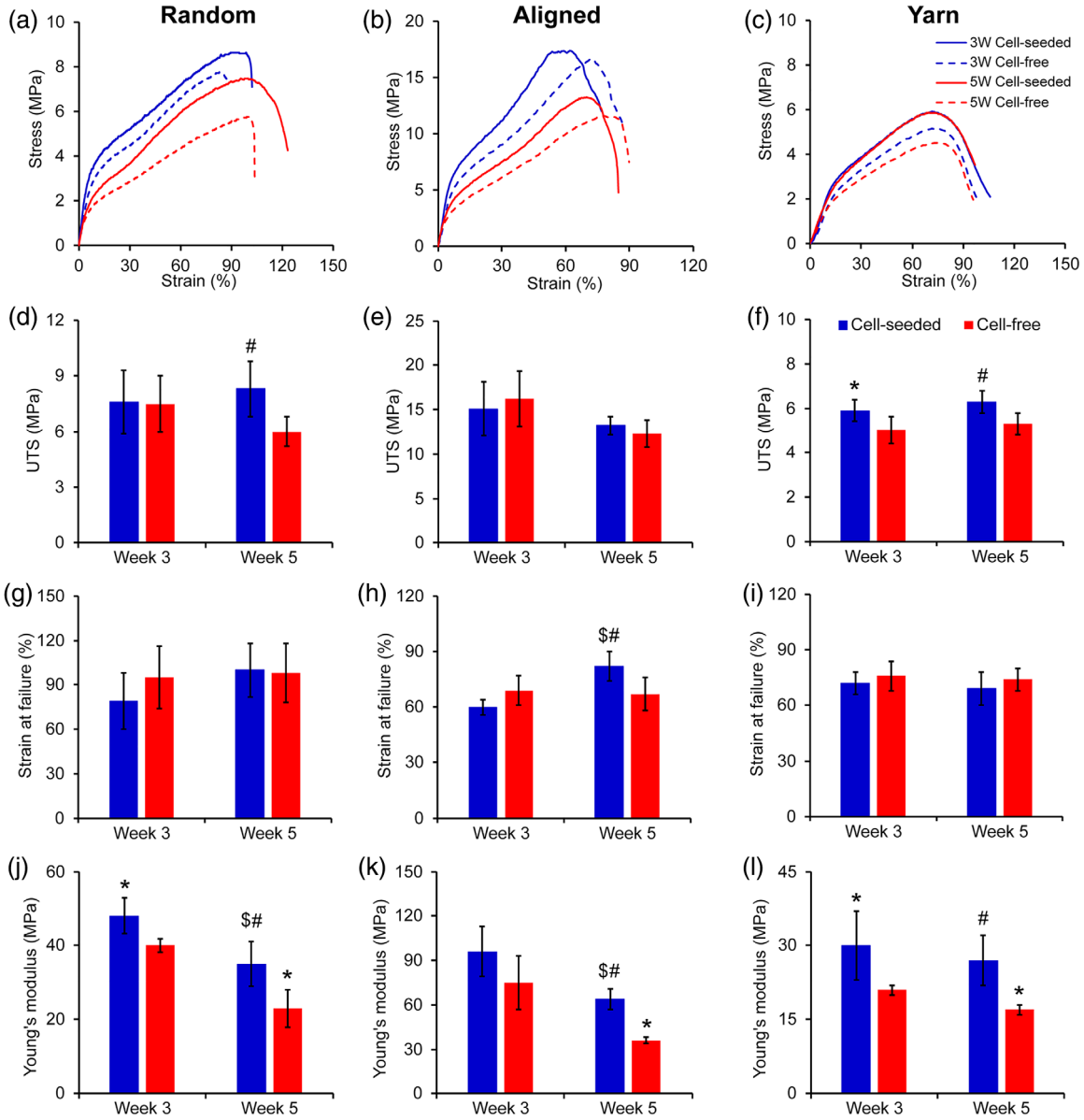

FIGURE 8 Tensile properties of cell-seeded scaffolds. Meniscus cell-seeded random (a) and aligned (b) scaffolds exhibit lower stress–strain curves from week 3 to week 5; cell-seeded yarn scaffold (c) retain comparable curves for up to 5 weeks. In addition, all cell-seeded scaffolds have higher curves than their corresponding cell-free scaffolds at each time point. The cell-seeded random (d) scaffold has a comparable UTS at week 3 and a significantly great UTS at week 5 compared with its cell-free control. The cell-seeded aligned scaffold (e) remains comparable UTS, while the cell-seeded scaffold (f) has significantly higher UTS in comparison with its cell-free control within 5 weeks. Meniscus cells have negligible effects on the breaking strains (g–i) but they significantly enhance Young's moduli (j–l) of electrospun scaffolds. Unpaired *t* test, $p < .05$, * versus 3 W cell-free, # versus 5 W cell-free, $ versus 3 W cell-seeded

demonstrated that the mechanical anisotropy of the meniscus is mainly dependent on its heterogeneous ECM structure.[8] Electrospinning is the simplest method to prepare nanofibrous scaffolds, by which the anisotropic characteristics of nanofibers can be feasibly manipulated by varying target collectors. In this study, we used a conventional electrospinning system to prepare random nanofibrous scaffolds (Figure 1b). The as-electrospun nanofibers are positively charged and deposit on the negatively charged plate in a random manner. This scaffold exhibits a smooth surface (Figure 2a) with random nanofibers (Figure 2d) and is bionic to the surface layer of the meniscus (Figure 1a). Collecting nanofibers via a high-speed rotating mandrel (Figure 1c) gives to a dense nanofibrous membrane (Figure 2b,e) that shares the same anisotropic feature with the superficial layer of the meniscus (Figure 1a). These results highlight the feasibility of electrospinning in producing both random and aligned nanofibrous scaffolds to reassemble the top and superficial layers of the meniscus, respectively.

The major structural unit of ECM that provides tensile strength along the circumferential direction is the highly organized collagen fibril bundles located in the deep zone of the meniscus. These circumferential bundles are wrapped up by transversely oriented collagen fibril sheets, namely, the radially aligned fibers of the superficial layer beneath the top surface (Figure 1a). Although electrospinning is effective in reproducing the surface and superficial layers of the meniscus,[16,32,33] it remains a significant challenge to recapitulate the ultrastructure of circumferential collagen fibril bundles. Similar to other soft tissues such as tendon[34] and ligament,[34,35] the dominant circumferential collagen fibrils of the meniscus are assembled in a reasonably homogeneous aligned manner into bundles (Figure 1a). This unique ultrastructure involves the self-assembly of collagen fibrils during individual development. In this study, we describe the technique of electrospinning with a dynamic collecting system that configures nanofibers into bundle-like yarns (Figures 1d and 2c,f,i), which replicates collagen fibril bundles of the meniscus. The mechanism underlying the formation of the bundle-like structure has been elucidated in our previous studies.[17,18] To our knowledge, this is the first report of an electrospun scaffold possesses biomimetic ultrastructure of circumferential collagen fibril bundles of the meniscus.

Many biomaterials including synthetic polymers such as PCL,[11,28,33] poly(lactic acid) (PLA),[31] poly(glycerol sebacate) (PGS),[16] and poly(lactic acid-co-glycolic acid) (PLGA),[36] as well as natural products including gelatin[36] and collagen,[37] either used in single formulation or their combinations, have been efforted to prepare nanofibrous scaffolds for meniscus tissue engineering. We selected the copolymer PLLA-CL for the current study because when processed into nanofibrous scaffolds via electrospinning, it shows greater mechanical strength than PCL[28] and is more flexible over pure PLA.[38] We introduced dmECM into PLLA-CL to improve the overall properties of scaffolds. The dmECM greatly increases the tensile strength when compared with pure PLLA-CL in our previous report.[39] This result agrees with a recent report by Gao et al that incorporation of dmECM into PCL reduces the hydrophobicity and increases mechanical strength.[28] The improved mechanical strength could be attributable to the increased crystallinity induced by the incorporated dmECM, which is highly desirable as it enables the scaffold with greater capacity to resist mechanical loading. Other reports also demonstrate the similar augment effects of natural polymers including collagen,[40] gelatin,[41] and silk fibroin[42] on synthetic polymers in terms of mechanical strengths. We used a solution with the PLLA-CL/dmECM ratio of 9:1 for this study because we found that nanofibers with higher contents of dmECM gradually lose their structural integrity when subject to continuous liquid disturbance (data not shown). The meniscus ECM has an anisotropic fibrous structure, thus its mechanical properties are largely depended on the orientation of the collagen fibril bundles. It should be noted that these electrospun scaffolds have UTSs of 7–15 MPa, which is much lower than native meniscus (100–300 MPa) in the circumferential direction.[43] Interestingly, electrospun scaffolds have comparable elastic modulus to native meniscus in the radial direction,[44] indicating that they might be served as wrapping materials for radial tear treatment.[45]

Electrospun nanofibers are highly conducive for cell growth and promote matrix synthesis of cells. We show that electrospun scaffolds are cytocompatible to meniscus cells and support cell adhesion and maintain good cell viability during 5 weeks of in vitro culture. Meniscus cells exhibit a flatten, polygonal morphology on the random scaffold, while they adapt to the aligned fibrous structures and elongate along the fiber direction on the aligned and yarn scaffolds, indicating that cells could recognize and respond to the various surface textures of scaffolds. Recent reports also revealed distinct organizations of meniscus cells on electrospun scaffolds with various anisotropic properties.[29-33] The capacity of an electrospun scaffold to support cell proliferation is predominantly determined by its ultrastructure and porosity. Electrospun scaffolds composed of densely compacted nanofibers only allow cell proliferation on their surface in a two-dimensional manner, therefore, showing lower capacity in supporting cell proliferation than electrospun porous scaffolds.[46] Our previous studies prove that electrospun yarn scaffolds support greater proliferation rates of cells with respect to conventional electrospun scaffolds.[17,18,21] However, in the current study, meniscus cells did not show higher proliferation rates on the yarn scaffold over the random and aligned scaffolds. We attribute this inconsistent finding to the inherent slower proliferative capacity of primary meniscus cells.[47,48] Meniscus cells still proliferate actively even after 5-week culture and, therefore, show synchronous proliferation rates on these scaffolds.

Cultivated cells are known to secrete extracellular matrix that profoundly contributes to the mechanical properties of scaffolds. Our data indicate that the mechanical properties of cell-seeded scaffolds trend to higher with respect to their corresponding cell-free scaffolds at every time point (Figure 8). This is consistent with recent studies reported by Baek et al, where human meniscus cells significantly enhanced tensile strengths and stiffness of electrospun scaffolds.[29,31] Interestingly, both Beak's and our studies find a relative difference of approximately 60% in tensile modulus between cell-seeded and cell-free scaffolds, while our data indicate an increase in tensile strength by meniscus cells is not as significant as Baek's results.[29] This is probably due to the seeding density of cells and the supplement of growth

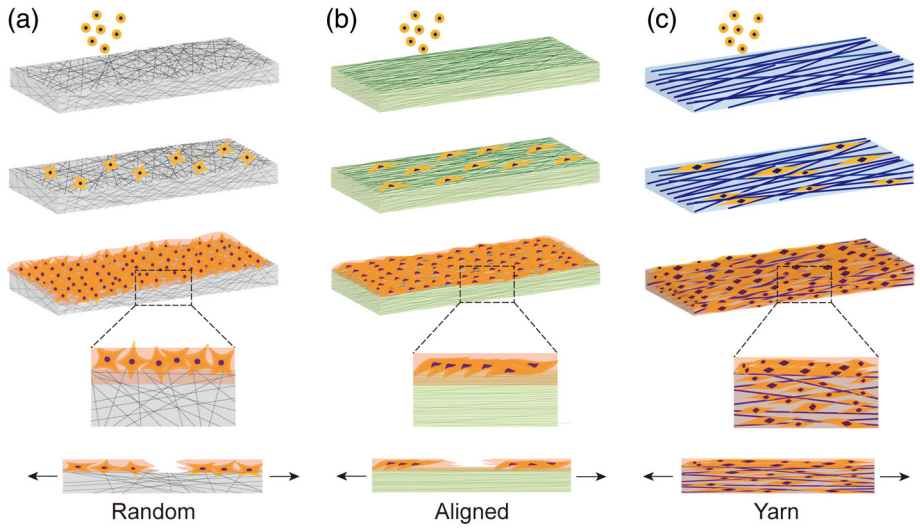

FIGURE 9 Schematic of meniscus cells growth on electrospun scaffolds. Both the random (a) and aligned (b) scaffolds have dense nanofibrous structures, which restrict cell proliferation only on the surface of scaffolds. The yarn scaffold has a porous fibrous structure and supports progressive cell infiltration (c). These distinct patterns of meniscus cells and their extracellular matrix deposition within scaffolds result in discrepant effects on mechanical properties of cell-seeded scaffolds: cells and matrix on the surface are not well incorporated with random and aligned scaffolds, therefore, not able to significantly increase the tensile strength of these scaffolds; meniscus cells disperse and produce extracellular matrix within the yarn scaffolds, thus generating reinforcement effects on the yarn scaffold

factors.[47-49] We seeded the scaffolds with much fewer cells and did not supplement any growth factors, which might be attributable to the slower proliferation of meniscus cells and extracellular matrix accumulation.

Although our data indicate that the increase of mechanical properties generated by meniscus cells is relatively small, it counteracts the mechanical loss of scaffolds caused by degradation to some extent. The reinforcement effect of the matrix generated by meniscus cells is somewhat dependent on the type of scaffolds. Both the cell-seeded random and aligned scaffolds showed decreased tensile moduli from week 3 to week 5 (Figure 8j,k), while the yarn scaffold did not experience loss in tensile modulus (Figure 8l). This discrepancy might be associated with the distribution of cells and their extracellular products within scaffolds. We find comparable numbers of cells on three scaffolds at each time point (Figure 5j), while their location within scaffolds was distinct as revealed by histological analysis (Figure 7). Herein, we propose a possible mechanism to illustrate how cell-scaffold interaction contributes to the mechanical properties of scaffolds (Figure 9). Meniscus cells proliferate and produce extracellular matrix but cannot penetrate densely compacted nanofibrous mesh, thus forming a thin layer on the surface of random (Figure 9a) and aligned (Figure 9b) scaffolds. This cell layer only contacts the surface of scaffolds and easily damages under stretch, therefore, it has limited reinforcement effects on the mechanical properties of scaffolds. In contrast, the yarn scaffold allows full penetration and even distribution of meniscus cells within the whole scaffold (Figure 9c). Meniscus cells attach to their surrounding nanofibers in a three-dimensional manner and come with extracellular matrix dispersed homogeneously within the yarn scaffold. In this scenario, meniscus cells and their extracellular matrix products integrate well with the yarn scaffold and form a tissue-like construct resembling the circumferential collagen bundles of the meniscus, thus greatly increasing the mechanical properties.

This study has some limitations. Although many groups demonstrated the feasibility of electrospinning to approximate distinct fibrous structures of meniscus ECM and herein we show three electrospun scaffolds with distinct fibrous organizations resembling the complex structures of the meniscus, it is still a huge challenge to construct a scaffold with meniscus-like geometry and hierarchical fibrous structures using electrospinning. Our future work will focus on the construction of such a biomimetic scaffold with appropriate geometry and size via a step-by-step electrospinning process. Combining electrospun nanofibers with hydrogels or dmECM might circumvent this problem.[31,32] We evaluated the potential of scaffolds with primary rabbit meniscus cells as many other reports did. While this is practicable for proof of concept studies, it is necessary to assess these scaffolds in a more clinically relevant manner, for example, using human meniscus cells derived from surgical debris[50] in our future study.

5 | CONCLUSIONS

We prepared electrospun scaffolds with distinct isotropic and mechanical properties, which approximate the hierarchical fibrous layers of meniscus ECM. These scaffolds are cytocompatible and support great growth of meniscus cells, especially, the yarn scaffold allows considerable cell infiltration. Meniscus cells proliferate and produce extracellular matrix within the yarn scaffold, generating tissue-like constructs in vitro. Future studies will integrate these individual

scaffolds into a single scaffold with hierarchical fibrous layers similar to that of the native meniscus.

ACKNOWLEDGMENTS

Funding was provided by Donghua University (Fundamental Research Funds for Central Universities 2232019D3-20), National Natural Science Foundation of China (31900949), and Science and Technology Commission of Shanghai Municipality (19440741300, 18490740400).

CONFLICT OF INTEREST

The authors declare no competing financial interests in this work.

AUTHOR CONTRIBUTIONS

Xiaoyu Wang and Jinglei Wu designed the study and wrote the manuscript. Xiaoyu Wang, Jingjing Zhu, Binbin Sun, Qiu Jin, and Haiyan Li performed the experiments. Xiaoyu Wang, Changlei Xia, Hongsheng Wang, Xiumei Mo, and Jinglei Wu analyzed and interpreted the data. All authors discussed the results and approved the final version of this article.

ORCID

Jinglei Wu https://orcid.org/0000-0001-9549-3992

REFERENCES

1. Baker P, Coggon D, Reading I, Barrett D, McLaren M, Cooper C. Sports injury, occupational physical activity, joint laxity, and meniscal damage. *J Rheumatol*. 2002;*29*(3):557-563.
2. Sweigart MA, Athanasiou KA. Toward tissue engineering of the knee meniscus. *Tissue Eng*. 2001;*7*(2):111-129.
3. Foad A. Self-limited healing of a radial tear of the lateral meniscus. *Knee Surg Sports Traumatol Arthrosc*. 2012;*20*(5):933-936.
4. McDermott I, Amis A. The consequences of meniscectomy. *J Bone Joint Surg*. 2006;*88*(12):1549-1556.
5. Salata MJ, Gibbs AE, Sekiya JK. A systematic review of clinical outcomes in patients undergoing meniscectomy. *Am J Sports Med*. 2010;*38*(9):1907-1916.
6. Lozano J, Ma CB, Cannon WD. All-inside meniscus repair: a systematic review. *Clin Orthop Relat Res*. 2007;*455*:134-141.
7. Andrews S, Ronsky J, Rattner J, Shrive N, Jamniczky H. An evaluation of meniscal collagenous structure using optical projection tomography. *BMC Med Imaging*. 2013;*13*(1):21.
8. Li Q, Qu F, Han B, et al. Micromechanical anisotropy and heterogeneity of the meniscus extracellular matrix. *Acta Biomater*. 2017;*54*:356-366.
9. Andrews SH, Rattner JB, Abusara Z, Adesida A, Shrive NG, Ronsky JL. Tie-fibre structure and organization in the knee menisci. *J Anat*. 2014;*224*(5):531-537.
10. Nöth U, Osyczka AM, Tuli R, Hickok NJ, Danielson KG, Tuan RS. Multilineage mesenchymal differentiation potential of human trabecular bone-derived cells. *J Orthop Res*. 2002;*20*(5):1060-1069.
11. Shimomura K, Bean AC, Lin H, Nakamura N, Tuan RS. In vitro repair of meniscal radial tear using aligned electrospun nanofibrous scaffold. *Tissue Eng Part A*. 2015;*21*(13–14):2066-2075.
12. Baker BM, Shah RP, Huang AH, Mauck RL. Dynamic tensile loading improves the functional properties of mesenchymal stem cell-laden nanofiber-based fibrocartilage. *Tissue Eng Part A*. 2011;*17*(9–10):1445-1455.
13. Bansal S, Mandalapu S, Aeppli C, et al. Mechanical function near defects in an aligned nanofiber composite is preserved by inclusion of disorganized layers: insight into meniscus structure and function. *Acta Biomater*. 2017;*56*:102-109.
14. Fisher MB, Henning EA, Söegaard N, Esterhai JL, Mauck RL. Organized nanofibrous scaffolds that mimic the macroscopic and microscopic architecture of the knee meniscus. *Acta Biomater*. 2013;*9*(1):4496-4504.
15. Martin JT, Milby AH, Ikuta K, et al. A radiopaque electrospun scaffold for engineering fibrous musculoskeletal tissues: scaffold characterization and in vivo applications. *Acta Biomater*. 2015;*26*:97-104.
16. Ifkovits JL, Wu K, Mauck RL, Burdick JA. The influence of fibrous elastomer structure and porosity on matrix organization. *PLoS One*. 2010;*5*(12):e15717.
17. Wu J, Huang C, Liu W, et al. Cell infiltration and vascularization in porous nanoyarn scaffolds prepared by dynamic liquid electrospinning. *J Biomed Nanotechnol*. 2014;*10*(4):603-614.
18. Wu J, Liu S, He L, et al. Electrospun nanoyarn scaffold and its application in tissue engineering. *Mater Lett*. 2012;*89*:146-149.
19. Liu S, Wu J, Liu X, et al. Osteochondral regeneration using an oriented nanofiber yarn-collagen type I/hyaluronate hybrid/TCP biphasic scaffold. *J Biomed Mater Res A*. 2015;*103*(2):581-592.
20. Xu Y, Dong S, Zhou Q, et al. The effect of mechanical stimulation on the maturation of TDSCs-poly(L-lactide-co-e-caprolactone)/collagen scaffold constructs for tendon tissue engineering. *Biomaterials*. 2014;*35*(9):2760-2772.
21. Xu Y, Wu J, Wang H, et al. Fabrication of electrospun poly(L-lactide-co-epsilon-caprolactone)/collagen nanoyarn network as a novel, three-dimensional, macroporous, aligned scaffold for tendon tissue engineering. *Tissue Eng Part C Methods*. 2013;*19*(12):925-936.
22. Zheng X, Wang W, Liu S, et al. Enhancement of chondrogenic differentiation of rabbit mesenchymal stem cells by oriented nanofiber yarn-collagen type I/hyaluronate hybrid. *Mater Sci Eng C*. 2016;*58*:1071-1076.
23. Chen Y-C, Chen R-N, Jhan H-J, et al. Development and characterization of acellular extracellular matrix scaffolds from porcine menisci for use in cartilage tissue engineering. *Tissue Eng Part C Methods*. 2015;*21*(9):971-986.
24. Schwarz S, Koerber L, Elsaesser AF, et al. Decellularized cartilage matrix as a novel biomatrix for cartilage tissue-engineering applications. *Tissue Eng Part A*. 2012;*18*(21–22):2195-2209.
25. Stapleton TW, Ingram J, Katta J, et al. Development and characterization of an acellular porcine medial meniscus for use in tissue engineering. *Tissue Eng Part A*. 2008;*14*(4):505-518.
26. Yuan Z, Liu S, Hao C, et al. AMECM/DCB scaffold prompts successful total meniscus reconstruction in a rabbit total meniscectomy model. *Biomaterials*. 2016;*111*:13-26.
27. Wu J, Ding Q, Dutta A, et al. An injectable extracellular matrix derived hydrogel for meniscus repair and regeneration. *Acta Biomater*. 2015;*16*:49-59.
28. Gao S, Guo W, Chen M, et al. Fabrication and characterization of electrospun nanofibers composed of decellularized meniscus extracellular matrix and polycaprolactone for meniscus tissue engineering. *J Mater Chem B*. 2017;*5*(12):2273-2285.
29. Baek J, Lotz M, D'Lima D. Core-shell nanofibrous scaffolds for repair of meniscus tears. *Tissue Eng Part A*. 2019;*25*(23–24):1577-1590.
30. Baek J, Sovani S, Glembotski NE, et al. Repair of avascular meniscus tears with electrospun collagen scaffolds seeded with human cells. *Tissue Eng Part A*. 2016;*22*(5–6):436-448.
31. Baek J, Chen X, Sovani S, Jin S, Grogan SP, D'Lima DD. Meniscus tissue engineering using a novel combination of electrospun scaffolds and human meniscus cells embedded within an extracellular matrix hydrogel. *J Orthop Res*. 2015;*33*(4):572-583.
32. Gao S, Chen M, Wang P, et al. An electrospun fiber reinforced scaffold promotes total meniscus regeneration in rabbit meniscectomy model. *Acta Biomater*. 2018;*73*:127-140.
33. Baker BM, Mauck RL. The effect of nanofiber alignment on the maturation of engineered meniscus constructs. *Biomaterials*. 2007;*28*(11):1967-1977.

34. Kannus P. Structure of the tendon connective tissue. *Scand J Med Sci Sports*. 2000;*10*(6):312-320.
35. Provenzano PP, Vanderby R. Collagen fibril morphology and organization: implications for force transmission in ligament and tendon. *Matrix Biol*. 2006;*25*(2):71-84.
36. Li P, Zhang W, Yu H, et al. Applying electrospun gelatin/poly (lactic acid-co-glycolic acid) bilayered nanofibers to fabrication of meniscal tissue engineering scaffold. *J Nanosci Nanotechnol*. 2016;*16*(5):4718-4726.
37. Baek J, Sovani S, Choi W, Jin S, Grogan SP, D'Lima DD. Meniscal tissue engineering using aligned collagen fibrous scaffolds: comparison of different human cell sources. *Tissue Eng Part A*. 2018;*24*(1–2):81-93.
38. Liu X, He X, Jin D, et al. A biodegradable multifunctional nanofibrous membrane for periodontal tissue regeneration. *Acta Biomater*. 2020; *108*:207-222.
39. Zhang K, Jinglei W, Huang C, Mo X. Fabrication of silk fibroin/P(LLA-CL) aligned nanofibrous scaffolds for nerve tissue engineering. *Macromol Mater Eng*. 2013;*298*(5):565-574.
40. Yin A, Zhang K, McClure MJ, et al. Electrospinning collagen/chitosan/poly(L-lactic acid-co-epsilon-caprolactone) to form a vascular graft: mechanical and biological characterization. *J Biomed Mater Res A*. 2013;*101*(5):1292-1301.
41. Kołbuk D, Sajkiewicz P, Maniura-Weber K, Fortunato G. Structure and morphology of electrospun polycaprolactone/gelatine nanofibres. *Eur Polym J*. 2013;*49*(8):2052-2061.
42. Zhang K, Wang H, Huang C, Su Y, Mo X, Ikada Y. Fabrication of silk fibroin blended P(LLA-CL) nanofibrous scaffolds for tissue engineering. *J Biomed Mater Res A*. 2010;*93A*(3):984-993.
43. Fithian DC, Kelly MA, Mow VC. Material properties and structure-function relationships in the menisci. *Clin Orthop Relat Res*. 1990;*252*: 19-31.
44. Warnecke D, Stein S, Haffner-Luntzer M, et al. Biomechanical, structural and biological characterisation of a new silk fibroin scaffold for meniscal repair. *J Mech Behav Biomed Mater*. 2018;*86*:314-324.
45. Shimomura K, Rothrauff BB, Hart DA, et al. Enhanced repair of meniscal hoop structure injuries using an aligned electrospun nanofibrous scaffold combined with a mesenchymal stem cell-derived tissue engineered construct. *Biomaterials*. 2019;*192*:346-354.
46. Wu J, Hong Y. Enhancing cell infiltration of electrospun fibrous scaffolds in tissue regeneration. *Bioact Mater*. 2016;*1*(1):56-64.
47. Gunja NJ, Uthamanthil RK, Athanasiou KA. Effects of TGF-β1 and hydrostatic pressure on meniscus cell-seeded scaffolds. *Biomaterials*. 2009;*30*(4):565-573.
48. Tumia NS, Johnstone AJ. Platelet derived growth factor-AB enhances knee meniscal cell activity in vitro. *Knee*. 2009;*16*(1):73-76.
49. Neves AA, Medcalf N, Brindle KM. Influence of stirring-induced mixing on cell proliferation and extracellular matrix deposition in meniscal cartilage constructs based on polyethylene terephthalate scaffolds. *Biomaterials*. 2005;*26*(23):4828-4836.
50. Baker BM, Nathan AS, Huffman GR, Mauck RL. Tissue engineering with meniscus cells derived from surgical debris. *Osteoarthr Cartil*. 2009;*17*(3):336-345.

How to cite this article: Wang X, Zhu J, Sun B, et al. Harnessing electrospun nanofibers to recapitulate hierarchical fibrous structures of meniscus. *J Biomed Mater Res*. 2020; 1–13. https://doi.org/10.1002/jbm.b.34692